Brief Communication

MOLECULAR METABOLISM

Beta-hydroxybutyrate dampens adipose progenitors' profibrotic activation through canonical Tgfβ signaling and non-canonical *ZFP36*-dependent mechanisms

Simon Lecoutre [1,4], Fatiha Merabtene [1,4], Elie-Julien El Hachem [1], Camille Gamblin [1], Christine Rouault [1], Nataliya Sokolovska [1], Hedi Soula [1], Wi S. Lai [2], Perry J. Blackshear [2], Karine Clément [1,3], Isabelle Dugail [1,*]

ABSTRACT

Background/Purpose: Adipose tissue contains progenitor cells that contribute to beneficial tissue expansion when needed by *de novo* adipocyte formation (classical white or beige fat cells with thermogenic potential). However, in chronic obesity, they can exhibit an activated pro-fibrotic, extracellular matrix (ECM)-depositing phenotype that highly aggravates obesity-related adipose tissue dysfunction.
Methods: Given that progenitors' fibrotic activation and fat cell browning appear to be antagonistic cell fates, we have examined the anti-fibrotic potential of pro-browning agents in an obesogenic condition.
Results: In obese mice fed a high fat diet, thermoneutral housing, which induces brown fat cell dormancy, increases the expression of ECM gene programs compared to conventionally raised animals, indicating aggravation of obesity-related tissue fibrosis at thermoneutrality. In a model of primary cultured murine adipose progenitors, we found that exposure to β-hydroxybutyrate selectively reduced Tgfβ-dependent profibrotic responses of ECM genes like *Ctgf*, *Loxl2* and *Fn1*. This effect is observed in both subcutaneous and visceral-derived adipose progenitors, as well as in 3T3-L1 fibroblasts. In 30 patients with obesity eligible for bariatric surgery, those with higher circulating β-hydroxybutyrate levels have lower subcutaneous adipose tissue fibrotic scores. Mechanistically, β-hydroxybutyrate limits Tgfβ-dependent collagen accumulation and reduces Smad2-3 protein expression and phosphorylation in visceral progenitors. Moreover, β-hydroxybutyrate induces the expression of the *ZFP36* gene, encoding a post-transcriptional regulator that promotes the degradation of mRNA by binding to AU-rich sites within 3′UTRs. Importantly, complete *ZFP36* deficiency in a mouse embryonic fibroblast line from null mice, or siRNA knock-down in primary progenitors, indicate that *ZFP36* is required for β-hydroxybutyrate anti-fibrotic effects.
Conclusion: These data unravel the potential of β-hydroxybutyrate to limit adipose tissue matrix deposition, a finding that might exploited in an obesogenic context.

Keywords Adipocyte; Progenitors; Fibrosis; Extracellular matrix

1. INTRODUCTION

Increasing fat mass over time favours progression to metabolic diseases and type-II diabetes. Maladaptive metabolism in obesity relies on chronic low-grade inflammation and subsequent disruption of insulin sensitivity [1]. It is linked to metabolic inflexibility of the expanded fat pads, which acquire features of a stiff, extracellular matrix-embedded fibrotic tissue, unable to sustain efficient lipid sequestration [2]. Adipose tissue (AT) fibrosis has strong deleterious impacts on glucose homeostasis, demonstrated in obese subjects [3,4] and in mouse models [5,6]. Conversely, thermogenic AT (brown or beige) is highly efficient in glucose uptake and lipid utilization [7,8], therefore a beneficial actor in blood glucose control [9,10]. Pathways controlling acquisition of a thermogenic fat cell phenotype are linked to the induction of a specific mitochondrial program dependent on PPARγ-associated transcriptional regulators like PRDM16 and PGC1a [11]. The recruitment of a pool of thermogenic adipocytes to target obesity-associated metabolic impairment has now become a therapeutical strategy under active research.

The source of brown-like and white adipocytes is a bulk of progenitors residing within the AT stroma-vascular fraction. The global adipose progenitor population has different propensities for beige/white adipogenesis, and can also develop into a pro-fibrotic fibroblastic phenotype, underlining a dual fibro/adipogenic potential highly

[1]Sorbonne Université, INSERM, Nutrition and obesities: systemic approach research group, Nutriomics, Paris F-75013. France [2]NIEHS, Durham, NC-27709, USA [3]Assistance Publique-Hôpitaux de Paris, Nutrition Department, Pitié-Salpêtrière Hospital, Paris 75013. France

[4] These authors are equally contributed.

*Corresponding author. E-mail: isabelle.dugail@inserm.fr (I. Dugail).

Received February 28, 2022 • Revision received May 2, 2022 • Accepted May 3, 2022 • Available online 9 May 2022

https://doi.org/10.1016/j.molmet.2022.101512

dependent on the tissue microenvironment. Although highly heterogeneous and yet incompletely characterized, the pool of AT progenitors (Cd31-, Cd45-) shares PDGFRa expression as a common cell surface marker [12]. Using this marker for functional progenitor targeting, we observed that fibrogenic responses to high fat diet, and fat browning potential of mouse subcutaneous adipose tissue, were inversely related pathways [6]. In line, another report demonstrated an inverse relationship between mouse fat browning and AT fibrosis, mediated by a PRDM16-dependent signal released from the adipocytes [13]. Thus, progenitors' fibrotic transformation and brown-like adipogenesis may involve antagonistic cell fates, associated with opposite consequences on whole body metabolic regulation.

A better understanding of how adipose progenitors orient cell choices towards fibrogenesis is essential for the development of new approaches to limit metabolic deterioration in obesity. A switch in the abundance of CD9-expressing visceral progenitors has been reported to promote pro-fibrotic activation [4]. It is also likely that the obese AT pro-inflammatory microenvironment triggers fibrogenesis at the expense of adipogenesis, linked to disruption in Tgfβ (Transforming growth factor) family members balance [14]. Moreover, the high demand for lipid storage in obesity might lead to preadipocytes premature exhaustion and senescence, precluding an adequate supply of new adipocytes [15].

In this study, we have explored the paradigm of pro-fibrotic versus adipogenic development of progenitors in the context of the obese AT. In particular, we demonstrate aggravated fibrosis in obese high fat diet-fed mice in which brown/beige fat dormancy is shaped by raising at thermoneutrality. We also demonstrate the anti-fibrotic properties of the fat browning factor β-hydroxybutyrate in primary Tgfβ-induced cultured progenitors from subcutaneous or visceral tissues. In addition to blunting of Smad/Tgfβ signalling by β-hydroxybutyrate in visceral progenitors, we unravel a novel mechanism linked to *ZFP36*/Tristetraprolin, a post-transcriptional regulator of mRNA stability, which is induced by β-hydroxybutyrate, and restrains fibrotic activation of subcutaneous progenitors.

2. MATERIALS AND METHODS

2.1. Materials

Collagenase A (R11088793001) was purchased from Roche, DMEM/Glutamax (61,965-026) from Gibco and foetal calf serum (CVFSVF00-01) from Eurobio Scientific. Sodium 3-β-Hydroxybutyrate (54,965) and L-(+)lactic acid (L1750) were obtained from Sigma. Tgfβ1 (human recombinant, ref 130-126-724) was from Myltenyi Biotech, Bmp4 (Human recombinant, ref PHC9534) from Invitrogen.

2.2. Patient studies

Human samples used were obtained from patients with obesity (N = 30, age 42.5±14.5, 10 men, 20 women, body mass index 44,0±6.5 kg/m^2) involved in the bariatric surgery program at the Nutrition Department of Pitié-Salpétrière hospital, France. Ten patients (7 women, 3 men) had normal glucose control, while the 20 others were either diabetic or glucose intolerant. Among diabetics, 4 were treated by GLP1 analogs, 2 by insulin, 5 by metformin. Six patients (3 men, 3 women) received statins to treat hyperlipemia. Eleven (7 women, 4 men) were on anti-hypertensive drugs. Blood samples were collected during preoperative hospital examination after an overnight fast. All patients received nutritional information and are encouraged to healthy diets. No specific diet pattern is recommended before surgery. Patients were part of a follow-up cohort with tissue bio banking during the surgery and beneficed fibrosis scoring of subcutaneous AT based on Picrosirius Red labelling of paraffin-embedded samples as described previously [16]. Briefly, label detection thresholds were adjusted with an image-analysis module using Calopix software (TRIBVN) and manual delimitation of red-stained AT, avoiding blood vessels and staining artifacts was performed. Label quantification was expressed as the ratio of red—stained to total tissue area. A combined semi-quantitative SCAT fibrosis score (FAT score) was then attributed to each patient according to the following rules: stage 0: no perilobular staining (thickness less than the diameter of average adipocyte) and no pericellular fibrosis (no accumulation of collagen around adipocytes localized in the depth of the AT lobules). Stage 3: severe paralobular fibrosis (thickness similar to the diameter of two average adipocytes) and severe paracellular fibrosis (thick labeling around adipocytes and presence of within label-trapped adipocytes). Ethical approval was obtained from the Research Ethics Committee of Hôtel-Dieu Hospital (CPP Ile-de-France N°1). Informed written consent was obtained from all subjects and the protocol was registered on http://www.clinicaltrials.gov (NCT01655017, NCT00476658). β-Hydroxybutyrate was measured on serum aliquots (5 μl) stored at −80C with a colorimetric assay kit (Abnova KA0854).

2.3. Mouse studies

Animal studies were conducted in agreement with ARRIVE guidelines, approved by local ethical committee (n°31,719). 4—6 week old C57Bl6/J mice were fed a high fat diet (Research Diet, D12492i) with free access to drinking water. They were housed (maximum of 5 mice per cage) at room temperature (22 °C) or at thermoneutrality (30 °C) in a climate chamber (TSE, PhenoMaster), with matched day—night light cycles and controlled humidity. Body composition was analyzed by nuclear magnetic resonance (Bruker Mouse Minispec, LF90). AT from visceral (gonadal), subcutaneous (inguinal) and interscapular brown fat (BAT) were frozen in liquid nitrogen or incubated with collagenase as described [6].

2.4. Primary cell culture

Six female mice fed on a standard chow diet were used for each cell preparation. Minced AT were incubated in collagenase dissociation medium for 30 min (visceral AT) or 1 h (Subcutaneous AT) under lateral shaking (100 rpm) at 37 °C. After filtration through a 100 μm cell strainer, medium was adjusted to 30 ml with PBS, cells were pelleted (10 min at 1500rpm), and suspended into 12 ml of DMEM/10% fetal calf serum. 0.5 ml was plated into 12-well culture plates in a 95%—5% air-CO_2 humidified atmosphere at 37 °C. After 4 h, non-attached cells were eliminated by 3 washes with PBS, and refed in fresh medium. The next day, all cultures were more than 80% confluent, and β-hydroxybutyrate (βOHB) (or other browning agents) was added alone 24 h prior to TGFb was introduced and maintained for additional 3 days. This combinatory treatment was defined to mimic the transition from a healthy pro-browning to a pro-fibrotic AT microenvironment.

2.5. Transfection with siRNA

Cells in DMEM 10% fetal calf serum were incubated with 20 nM siRNA duplexes (SR426376) or control scrambled sequences (SR0003) from Origene, using the lipofectamine RNAiMax transfection reagent (ref 13,778- Invitrogen). Cell treatment with effectors was performed on the next day in fresh medium.

2.6. *ZFP36*-deficient mouse fibroblasts

Cell line and its matched WT control line were originally derived from *ZFP36* −/− and +/+ embryos [17], and were cultured in DMEM high

glucose medium containing 1% penicillin/streptomycin and 10% fetal calf serum.

2.7. Gene and protein expression

Total RNA was extracted using RNeasy Mini kit (Qiagen, 74,104), and 500 μg was used for reverse transcription, followed by Quantitative real-time PCR using SyBr Green Master Mix (Applied Biosystems). All primer pairs were validated with cDNA calibration curves and a unique amplification product. For protein analysis, lysates in RIPA buffer (Sigma Aldrich, R0278) containing proteinase inhibitors (Complete Mini, Roche) were prepared (Bertin Technologies, Precellys 24) and cleared for 10 min at 10,000 rpm. Protein concentration was measured (ThermoFisher Scientific, BCA assay). Western blotting was performed as described [18].

2.8. Bioinformatics

We downloaded six data sets from publicly available reports [19–21] detailing information from chow-fed mice of different sexes, developmental states or adipose tissue anatomical locations. To keep a global overview of all datasets, we did not remove any genes from any of the six datasets, and kept all mitochondrial genes. In order to combine several scRNAseq experiments from different mouse studies while minimizing batch effects, we used Batch balanced K nearest Neighbours method (BBKNN) [22] available in the Scanpy Package to convert the distance between members of the same cluster into projectable connectivity. We then performed a Leiden Clustering (https://www.nature.com/articles/s41598-019-41695-z), which defined groups with similarity relationships. For each cluster, a ranking of genes defining the cluster was established. Based on a list of genes, we looked at the normalized expression of these genes in each of the clusters and performed stacked violin plots.

2.9. Statistical analysis

Cell culture experiments were performed in triplicate wells, repeated at least three times with independent cell preparations. Mean values from independent experiments were compared by Student's t test with a significance threshold at $p < 0.05$. In mouse experiments, differences in mean values from individual mice (6–10 per group) were evaluated by Student's *t* test. Spearman correlations were considered significant when $p < 0.05$.

3. RESULTS

3.1. Thermogenic fat dormancy by thermoneutral housing aggravates obesity-dependent extracellular matrix (ECM) gene expression in mouse AT

Cold exposure that activates beige adipocyte biogenesis reduces adipose tissue fibrosis and improves systemic glucose homeostasis in mice [5,23]. To examine if shutting down of thermogenic activity could reciprocally increase the severity of high fat diet (HFD)-induced AT fibrosis we compared HFD mice (both sexes) housed at either thermoneutrality (TN, 30 °C) or room temperature (RT, 20–22 °C). While pre- or post-HFD mean body weights did not significantly differ between groups (Suppl Fig. 1A), TN female mice gained more weight than RT females, close to growth rates of RT males (Suppl Fig. 1B). Moreover, 9 weeks on HFD at TN instead of RT significantly increased fat mass in female mice (Suppl Fig. 1C). Thus, TN housing combined with HFD amplified fat accretion, more markedly in females than in males.

Compared to their conventionally raised counterparts fed HFD, TN mice expressed lower levels of BAT *Ucp1* mRNA (Figure. 1A), and developed more inflamed BAT, with higher expression of *Il6*, *Tnfα* and *Cd68* (Figure. 1B). Moreover, a number of genes involved in ECM development were overexpressed in TN compared to RT. Specifically, TN enhanced genes encoding fibrillary collagens (*Col1a1*, and *Col3a1)*, ECM modifying enzymes such as *Loxl2* (a collagen/elastin crosslinker), and the matrix metalloproteinase regulator *Timp1* (Figure. 1C) which are implicated in the development of AT fibrosis [24]. Interestingly, BAT *Ucp1* negatively correlated with *Col1a1* and *Col3a1* expression (Figure. 1D). Comparison of BAT histology showed bigger lipid droplets in TN mice, as expected (Figure. 1E). At low magnification, we noticed the presence of prominent white spans formed with a-cellular material indicative of deposited extracellular matrix delimiting lobules in TN BAT. Semi-quantitative analysis showed significantly increased number of lobules in TN compared to RT samples (Figure. 1F). Thus, TN housing amplified the HFD-dependent ECM gene fibrotic program and matrix deposition in BAT.

In subcutaneous fat (SCAT), we found increased collagen1 protein content in TN versus RT mice (Figure. 1G). Although the topology of collagen accumulation in TN mice SCAT was not determined in the present study, we previously observed that HFD mice at RT preferentially accumulated collagen as perilobular fibrosis [6]. SCAT is a depot in which conventional white and brown-like fat cells are mixed, resulting in highly variable *Ucp1* mRNA expression among individual mice. A lower proportion of TN mice expressed high (above median) *Ucp1* mRNA, indicating a reduced propensity for SCAT beiging at TN (Figure. 1H). Among SCAT expressing *Ucp1* above the median, *Ucp1* mRNA negatively associated with *Col3a1* and *Fn1* (Figure. 1I). Thus, thermoneutral housing of mice showed an Ucp1-dependent inverse link to ECM gene patterns, which is consistent with antagonistic regulation of fibrotic and browning programs.

3.2. Reciprocal beiging and fibrotic responses of progenitors in a simplified culture system

As AT resident progenitors are a common source of both beige fat cells or profibrotic fibroblasts, we aimed to establish a simplified *in vitro* system to investigate fibrotic versus beige fat development. We used the stroma-vascular cell fraction of mouse AT from subcutaneous (SCAT) or visceral (VAT) fat depots, known to exhibit common susceptibility but distinct efficiencies for beiging or fibrotic development *in vivo*. Considering high heterogeneity of adipose progenitor cell population revealed by single cell sequencing [19–21], we aimed to minimize any drift in relative abundance of progenitor subsets that might occur during *in vitro* propagation. Cells recovered from collagenase digestion were plated at high density (80% confluence after 4-hour attachment), which ensured minimal proliferation and limited composition shifts from potential differences in proliferative rates among progenitor subtypes. Moreover, only primary first-passage cells were used, and culture duration did not exceed 5 days.

In this system, we tested cell responses to the canonical pro-fibrotic agent Tgfβ, as well as to previously characterized browning factors, i.e., β-hydroxybutyrate (βOHB) and Bone Morphogenic Protein 4 (Bmp4) [13,25]. All progenitors responded to Tgfβ exposure by marked morphological changes, with elongated cell shapes and dense cell–cell contacts (Suppl Fig. 2A). As expected, pro-fibrotic Tgfβ treatment upregulated the expression of ECM marker genes (i.e. *Col1a1*, *Ctgf*, *Loxl2)* in progenitors derived from either visceral (Suppl Fig. 2B) or subcutaneous (Suppl Fig. 2C) fat. *Fn1* (encoding the abundant matrix protein fibronectin) and *Col3a1* mRNAs were up-regulated by Tgfβ in visceral progenitors only. We also observed that lactate addition in the culture medium stimulated ECM gene expression, with synergistic effect to Tgfβ.

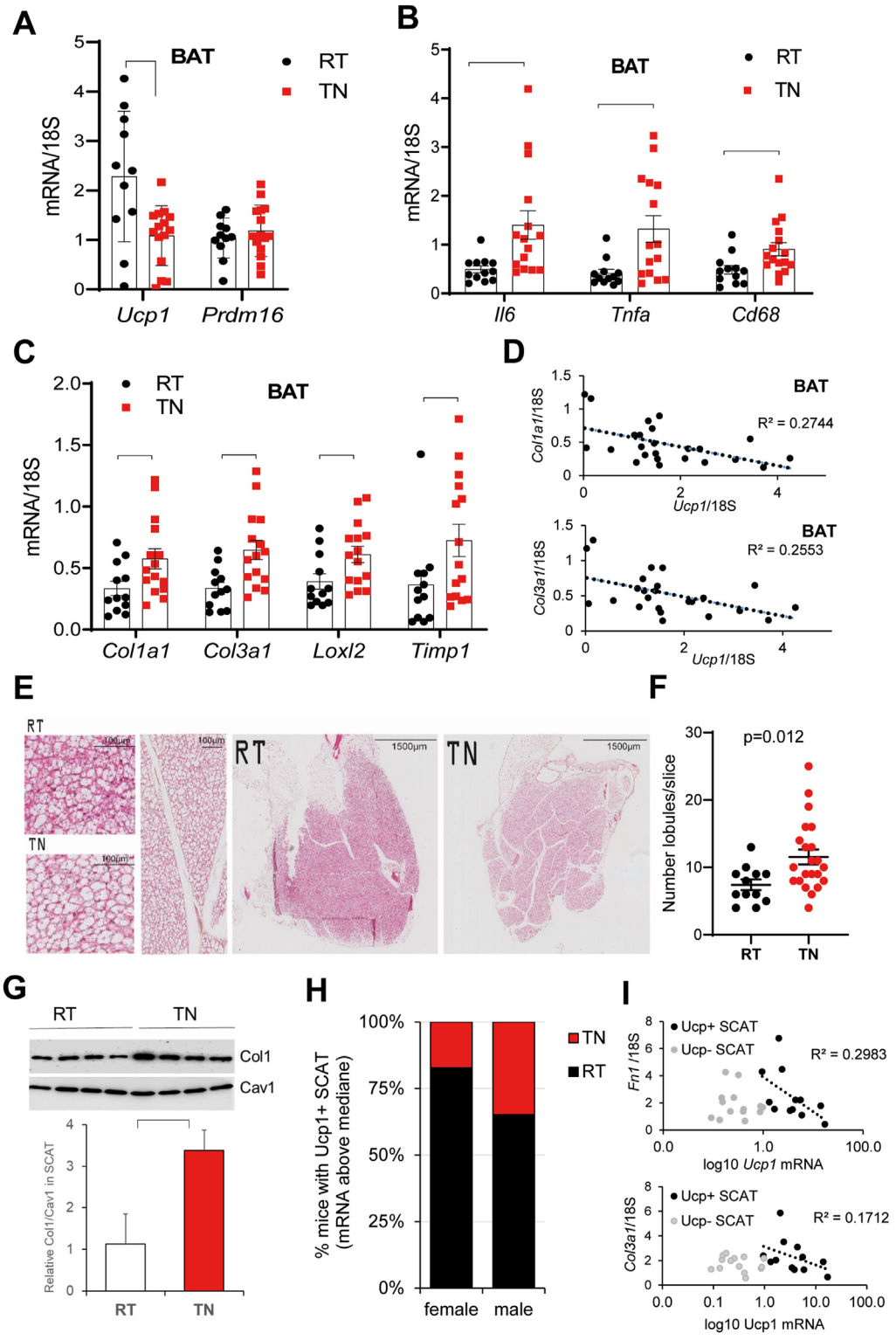

Figure 1: *Thermoneutral housing aggravates HFD-induced adipose tissue ECM gene program in mice.* Mice were housed for 9 weeks at room temperature (RT, 22 °C) or, thermoneutrality (TN, 30 °C) and received ad libitum HFD feeding. **A-D:** Brown adipose tissue (BAT) gene expression after 9 weeks on HFD was evaluated by Real time Q-PCR and normalized to 18 S. Values from individual mice are plotted, parentheses indicate significant differences between groups assessed by Student's t test. **E:** Hematoxilin/eosin BAT slices from RT and TN mice at different focus level (see scale bar in each image). Left panels show increased lipid droplet size in TN compared to RT (left panels). White spans consisting of acellular material (vertical image) were identified in whole tissue scans, delimiting lobules. **F:** Semi quantitative analysis of lobule number. Each point is from individual mice. **G:** Western blot analysis of SCAT Collagen1 content in RT and TN mice. Four tissues from individual mice are shown in each group; signals are normalized to Caveolin 1 for quantification. Parenthesis indicates significant difference ($p < 0.05$) by t test. **H:** Proportion of mice with Ucp1 positive SCAT (defined as above median *Ucp1* mRNA value) in RT and TN groups. P value = 0.035 by Chi2 Test **I:** Correlation between Ucp1 expression in SCAT and ECM genes (*Fn1*: upper panel, Col3a1: lower panel). Significant correlation ($p < 0.05$) is found in Ucp1+ SCAT (black) but not Ucp1- SCAT (grey). (For interpretation of the references to colour in this figure legend, the reader is referred to the Web version of this article.)

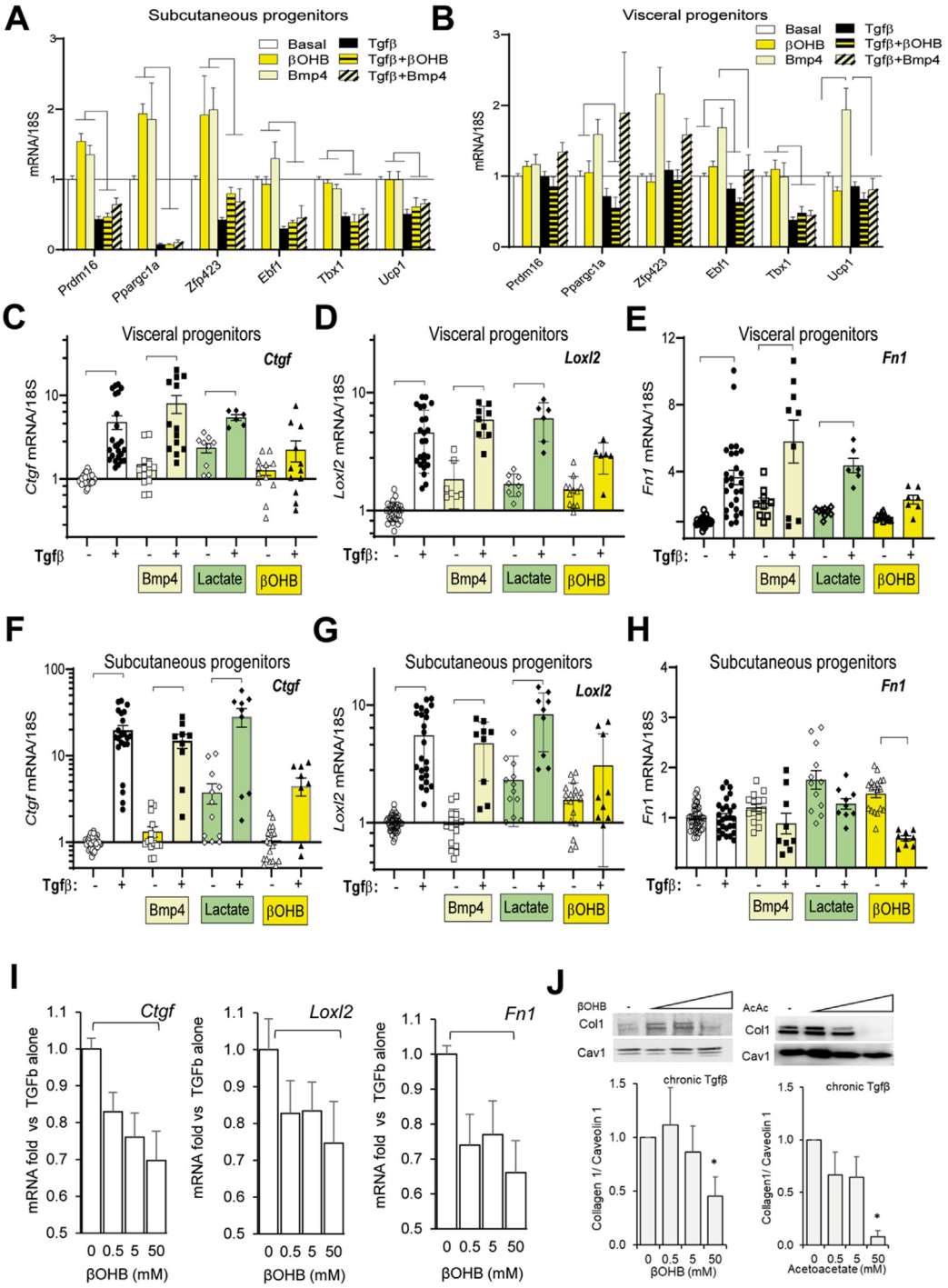

Figure 2: *βOHB counteracts Tgfβ-mediated stimulation of ECM genes.* Combinatorial treatment with browning agents and Tgfb of visceral **(A)** or subcutaneous progenitors **(B)** on the expression of browning genes. βOHB (50 mM) or Bmp4 (10 ng/ml) was added 24 h after plating and Tgfβ (10 ng/ml) was added the following day, until day 5. Bars are mean+/- sem of three independent cell preparations. The same experimental scheme was used in **(C–H)**, to assess *Ctgf*, *Loxl2* and *Fn1* mRNA responses. Each point is an individual well from triplicates in at least 4 independent cell preparations. **I:** Dose-dependent response of *Ctgf*, *Loxl2* and *Fn1* gene expression to βOHB in the presence of Tgfβ in primary subcutaneous progenitors. Parentheses indicate significant differences between conditions, by Student's t test. **J:** Western blot analysis of Collagen1 protein expression in Tgfβ-stimulated visceral progenitors in the presence of βOHB or Acetoacetate. βOHB or Acetoacetate was added 1 day post plating and was maintained until cell harvest (Day 5). Chronic Tgfβ stimulation started from Day 2 to Day 5. Collagen1 antibody was from Proteintech, ref14695-1. Representative blot is shown, with quantification from 2 to 4 independent cell preparations.

As expected, progenitor response to browning agents depended on fat tissue origin. Indeed, visceral progenitors (Suppl Fig. 2D) responded to Bmp4 by inducing *Ppargc1a* mRNA, a master regulator of the mitochondrial program, as well as *Zeb1*, *Zfp423*, *Ebf1* and *Ucp1*. βOHB treatment had limited effects on visceral progenitors and only slightly increased *Zeb1* mRNA. Subcutaneous progenitors (Suppl Fig. 2E)

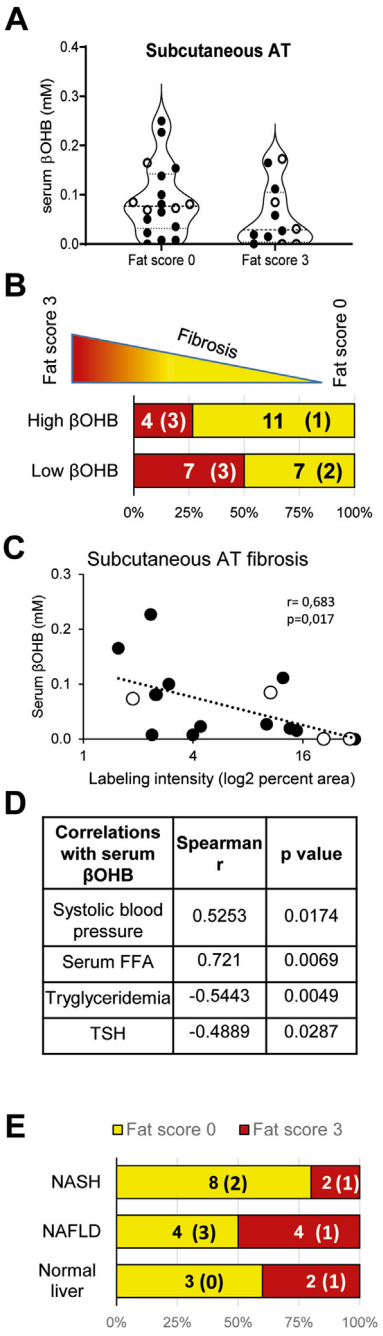

Correlations with serum βOHB	Spearman r	p value
Systolic blood pressure	0.5253	0.0174
Serum FFA	0.721	0.0069
Tryglyceridemia	-0.5443	0.0049
TSH	-0.4889	0.0287

Figure 3: *Serum βOHB levels negatively associate with subcutaneous adipose tissue fibrosis in patients with obesity.* **A:** Serum βOHB levels were assessed in a group of 29 obese patients eligible for bariatric surgery, in which the intensity of subcutaneous fat fibrosis had been scored as previously described. Men are represented as open symbols. **B:** Patient stratification according to serum βOHB (relative to median value) indicates preferential clustering of patients with low Fat score in the high βOHB group. Numbers represent the total number of patients in stratification groups, with the number of men in parenthesis **C:** Negative association (Spearman correlation) of serum βOHB levels and intensity of ECM labelling by Picrosirius-red in histological biopsies of subcutaneous adipose tissue in a subgroup of 16 patients. Open symbols are men. **D:** Association of clinical parameters to serum βOHB levels in the patients studied. **E**: Patients distribution according to Fat score and biopsy-proven liver status. Numbers represent the total number of patients in stratification groups, with the number of men in parenthesis. (For interpretation of the references to colour in this figure legend, the reader is referred to the Web version of this article.)

induced *Prdm16*, *Ppargc1a* and *Zfp423* when exposed to either βOHB or Bmp4, but displayed marginal responses in other markers. Noteworthy, in this experiment, no adipocyte differentiation cocktail was applied and progenitors were maintained for only 5 days, which might explain partial up-regulation of the browning gene program.

As a whole, these data confirm the dual potential of primary cultured progenitors to respond to browning and pro-fibrotic agents, mirroring the *in vivo* situation. Noticeably, although constitutive stimulation of the PDGF receptor was shown to activate fibrotic development of progenitors in multiple mouse tissues *in vivo* [26], we could not detect pro-fibrotic responses to PDGF-A in cell culture (Suppl Fig. 2F-G), likely because PDGF receptor expression/function might be compromised by collagenase digestion or *in vitro* cell maintenance.

3.3. βOHButyrate counteracts Tgfβ stimulation of ECM genes and is anti-fibrotic

Next, progenitors were exposed to βOHB or Bmp4 alone for 24 h prior to addition of Tgfβ in combination with the browning agent for the following three days. We found that Tgfβ diminished expression of beige adipocyte markers in subcutaneous progenitors, alone or with βOHB or Bmp4 co-exposure (Figure. 2A). The anti-browning effect of Tgfβ over βOHB was also seen in visceral progenitors, although less marked and mostly restricted to *Tbx1 and Ppargc1a* mRNAs (Figure. 2B). By contrast, *Ppargc1a* and *Zfp4*23 mRNAs were not suppressed by Tgfβ in Bmp4-stimulated visceral cells. Thus, Tgfβ selectively inhibits βOHB-dependent beiging.

We then examined if browning agents had the ability to counteract Tgfβ-dependent fibrotic response. βOHB (but not Bmp4) abolished *Ctgf* and *Loxl2* mRNA induction by Tgfβ in subcutaneous and visceral cells (Fig. 2CD-FG). *Fn1* gene induction by Tgfb in visceral progenitors was also attenuated by βOHB specifically (Figure. 2E), and the βOHB/Tgfβ combination significantly lowered *Fn1* in subcutaneous progenitors while Tgfβ alone did not produce stimulation (Figure. 2H).

In vivo, βOHB circulating concentrations change from a physiological range (0.1—0.5 mM) to more than 1 mM in fasting subjects, and rise up to 10 mM or more in diabetes. βOHB blunted Tgfβ-stimulated *Ctgf*, *Loxl2* and *Fn1* mRNA expression of primary progenitors in a dose dependent manner (Figure. 2I). Noticeably, in the fibroblastic 3T3-L1 cell line committed to adipogenesis, we also observed attenuated *Ctgf* mRNA induction in the combined presence of Tgfβ and βOHB compared to Tgfβ alone (Suppl Fig. 3A). Thus, βOHB can counteract pro-fibrotic action of Tgfβ in progenitors, independent of their tissue origin. Attenuation by βOHB of Tgfβ-dependent gene expression translated into lower Collagen1 protein contents, an effect shared with Acetoacetate, a closely βOHB-related ketone body (Figure. 2J).

To examine if the anti-fibrotic action of βOHB might have some relevance *in vivo*, we examined serum βOHB concentrations in a group of 30 patients with obesity involved in a bariatric surgery program, in which SCAT fibrosis was graded according to a previously defined "Fat score" integrating pericellular and perilobular tissue fibrosis, as described in [16]. Despite a similar degree of obesity in this small-sized cohort, a trend towards lower serum βOHB was found in those with higher Fat scores (Figure. 3A). After stratification on βOHB levels (median = 0.067 mM), equal distribution among highly fibrotic or non-fibrotic AT was observed in the low βOHB group, a proportion that fell to 25/75 in patients with high βOHB (Figure. 3B). Quantitative picrosirius red labelling indicated negative correlation with serum βOHB concentrations (Figure. 3C), consistent with an anti-fibrotic role of βOHB *in vivo*. Serum βOHB regulation obviously extends beyond AT fibrosis. In agreement, we observed that βOHB levels positively

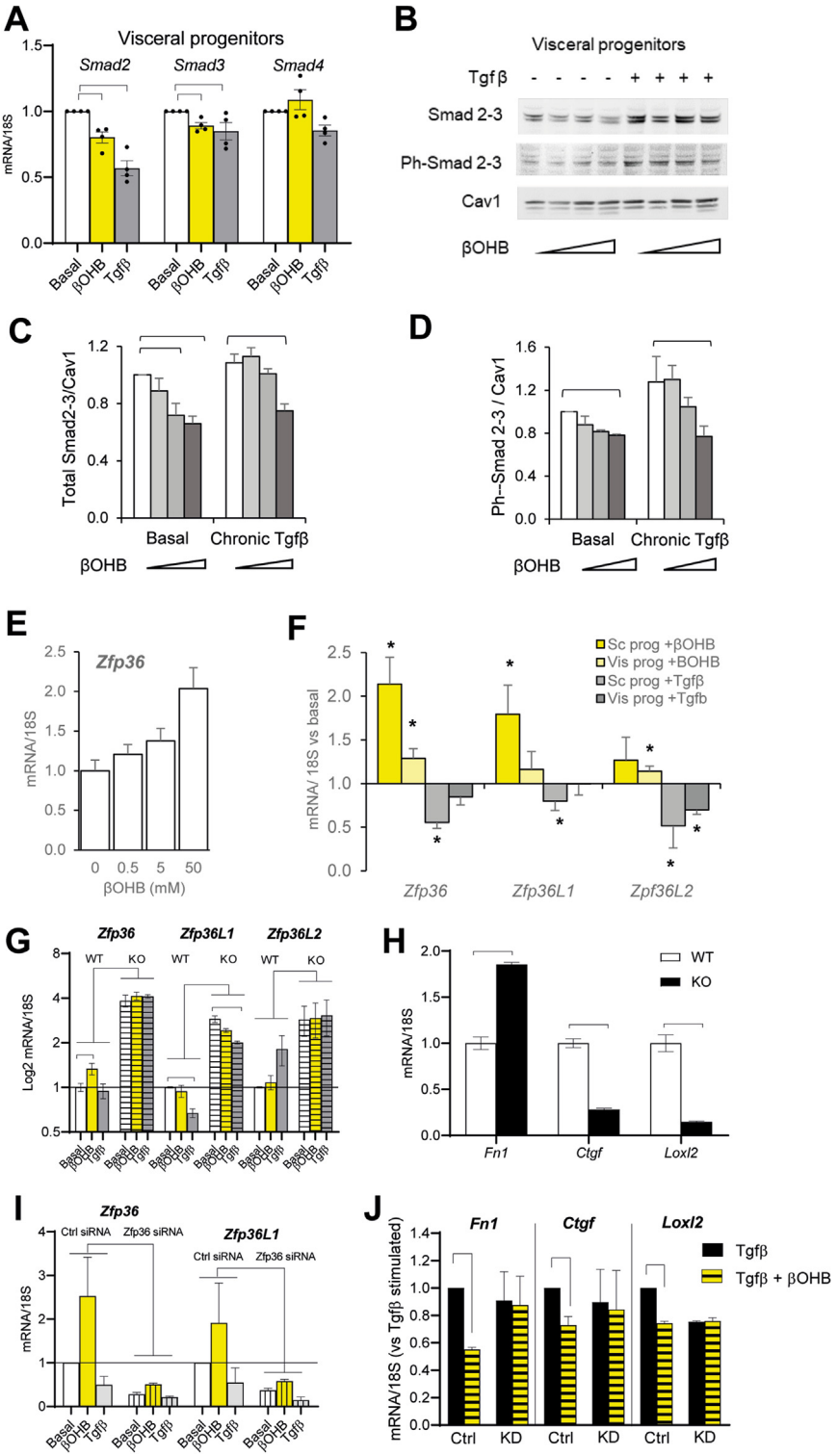

Figure 4: *Mechanisms of fibrotic attenuation by βOHB.* ***A:*** Smads mRNA expression in the presence of βOHB or chronic Tgfβ. Bars are mean values ± sem from 4 independent cell preparations. **B:** A representative western blot probed with antibodies against Smad2-3 (Cell signalling, ref 8685), Phospho Smad2 (Ser465/467)/Smad3 (Ser423/425) (Cell signalling, ref 8828 and Caveolin 1 (BD Transduction Laboratory, ref 610,060). *βOHB* concentration range is as in Figure 1, in the presence or absence of a chronic Tgfβ stimulation. **C-D**: Quantitative analysis of protein signal intensity after normalization with Caveolin-1 as a loading control. Bars are mean values from 3 independent cell preparations. Parentheses indicate significant differences between groups by t test. **E:** *ZFP36* mRNA upregulation by βOHB. **F:** Expression of *ZFP36* and related transcripts by βOHB and Tgfβ in subcutaneous and visceral progenitors. Bars are mean values ± sem from 3 to 5 independent cell preparations. * indicate significant differences compared to basal by Student t test. **G—H:** Gene expression in fibroblast cell lines from Wild Type (WT) or *ZFP36* KO mice. Note that in KO mice, *ZFP36* mRNA is transcribed but contains an insertion in exon 2 which prevents protein production. **I-J:** Knock-down of *ZFP36* with siRNA in primary progenitors maintained with Tgfβ with or without βOHB. Bars are mean values from 3 independent experiments. Parentheses indicate significant differences between groups by *t* test.

correlated with serum free fatty acids or systolic blood pressure, and negatively associated to triglyceridemia and thyroid stimulating hormone (Figure. 3D). The results were not influenced by gender. Regarding liver status that could be documented from a liver biopsy in 25 patients of the cohort, no link was found between Fat score and liver fibrosis. An equal proportion of adipose tissue samples were scored for high or low fat fibrosis among patients with normal liver histology or non-alcoholic fatty liver disease (NAFLD). Even, in 10 patients with biopsy-proven non-alcoholic steato-hepatitis (NASH), only 2 had elevated Fat score, whereas 8 had non-fibrotic fat tissue (Figure. 3E).

3.4. Mechanisms of βOHButyrate anti-fibrotic activity by canonical SMAD signalling and non-canonical ZFP36 induction

3.4.1. βOHButyrate reduces smad activation in visceral progenitors

βOHB is metabolized into acetylCoA that enter the TCA cycle. We reasoned that if βOHB metabolism was involved, its impact should be stronger in conditions of carbon sources limitation. Progenitors were cultured in Gln High, a high glucose, glutamine-supplemented medium, or in Gln Low, a high glucose, glutamine-depleted medium, in which glutamine was only available from serum. Such reduced glutamine/high glucose conditions the AT microenvironment found in obese diabetic subjects, as described [27]. We observed that βOHB equally attenuated Tgfβ-dependent elevation of *Ctgf* mRNA in low or high Gln (Suppl Fig. 3B), suggesting that modulation of carbon entry in the TCA cycle is not a major contributor of βOHB anti-fibrotic effect.

Tgfβ regulates the expression of ECM genes by activation of SMAD-2/3 downstream of Tgfβ receptors [28]. We firstconsidered that anti-fibrotic βOHB might act at the pre-receptor level by production of extracellular modulators able to restrain ligand binding or presentation [29]. However, exposure to a *bona fide* exogenous Tgfβ antagonist, follistatin, alone or in combination with βOHB, had no effect on visceral progenitors ECM gene expression (Suppl Fig. 3C). We next examined SMAD-2/3 regulation, whose phosphorylation on serine residues 423—426 is induced downstream of Tgfβ receptor. We observed that *Smad2* and *Smad3* mRNAs were slightly but significantly reduced by βOHB treatment in, whereas *Smad4* mRNA did not change (Figure. 4A). Western blots confirmed a dose-dependent decrease (30—40%) of Smad-2/3 protein contents upon βOHB exposure, in both unstimulated cells or after chronic Tgfβ stimulation (Figure 4B,C). Moreover, SMAD-2/3 serine phosphorylation was reduced in chronically Tgfβ treated visceral progenitors (Figure. 4D). Thus, blunting of Smad-2/3 dependent Tgfβ signalling by βOHB likely contributes its anti-fibrotic response. However, in similar experiments with subcutaneous progenitors, Smad-dependent Tgfβ response was not significantly affected by βOHB (data not shown), suggesting additional mechanisms might operate depending on cell origin.

3.4.2. Identification of *ZFP36* as a mediator of βOHB anti-fibrotic action

To identify other βOHB-driven mechanisms, we explored data generated from single cell RNA sequencing studies, which document specific AT stromal gene expression in progenitor subgroups. From publicly available reports [19—21], data sets detailing information from chow fed mice at different developmental states, AT anatomical locations or sex were downloaded, integrated using Batch Balanced K-nearest Neighborhood algorithm (https://doi.org/10.1093/bioinformatics/btz625), and processed by Leiden clustering for community detection (https://doi.org/10.1038/s41598-019-41695-z), which defined groups with similarity relationships. We found that *Fabp4*, *Cd36*, *Pparg* and *Cav1* genes, associated with adipogenesis, top ranked in three clusters, likely preadipocyte subsets at different stages (Suppl Fig. 4A). Using the ranked gene list to define group identity, we preselected a cluster comprising top ranking expression of ECM related genes (*Col1a1*, *Col3a1*, *Gsn*, *Dcn*) and the progenitor gene marker *Pdgfra*. This progenitor cluster with high potential for ECM deposition also contained Tgfβ receptor genes, suggesting responsiveness to pro-fibrotic factors. A top ranked gene in this cluster was *ZFP36*, which encodes a protein known as Tristetraprolin (TTP), a member of the "early response gene" family closely related to *ZFP36*L1 and *ZFP36*L2. *ZFP36* proteins belong to a family of RNA binding proteins known to destabilize AU—rich element (ARE)—containing mRNAs by promoting the removal of their polyA tails [30]. Indeed, *ZFP36* was found to decrease the stability of anti-adipogenic *Tnfa* mRNA, and *ZFP36*L1 could target inflammatory transcripts of numerous components of senescence-associated secretory phenotype.

Search in ARED-Plus (http://brp.kfshrc.edu.sa/ared), the AU-Rich Element Database [31] revealed hits in the 3′UTRs of *Ctfg* and *Fn1* mRNAs, making *ZFP36* an attractive candidate regulator of ECM transcript stability. Moreover, a survey of *ZFP36* expression patterns from public databases indicated preferential expression of *ZFP36* mRNA, and related *ZFP36l1* and *ZFP36l2* in BAT versus white fat (GSE 8044), while in GSE40486, BAT *ZFP36* was induced by cold (Suppl Fig. 4B). High-throughput studies in T cells highly expressing *ZFP36*, to identify direct targets by sequencing UV crosslinked immunoprecipitated transcripts, revealed hundreds of mRNAs to which *ZFP36* could bind [32], among which Glutaminase (encoded by Gls gene). Functionally, glutaminolysis is a pathway that feeds proline synthesis, a highly abundant amino acid in collagens. Thus, links from glutaminase to collagen deposition through *ZFP36* has functional relevance. We found that Tgfβ stimulated *Gls* expression more than 3-fold in 3T3-L1 preadipocytes, an effect that was completely blunted by the βOHB/Tgfβ combination (Suppl Fig. 3D). Such a similarity in the regulation of *Gls*, a *bona fide ZFP36* target, with that of *Ctgf*, and *Fn1*, bearing potential *ZFP36* binding sequences, reinforced the possibility that these might be under *ZFP36* post-transcriptional control.

Consistent with a role for *ZFP36* in βOHB anti-fibrogenic effects, we found that primary subcutaneous progenitors *ZFP36* mRNA dose-dependently increased (2-fold) upon βOHB exposure (Figure. 4E). βOHB also stimulated the expression of the closely related *ZFP36l1* and *ZFP36l2* (Figure. 4F). Conversely, pro-fibrotic stimulation with Tgfβ, in which optimal stability of ECM transcripts is expected, led to a significant drop in *ZFP36* and related *ZFP36l1 and 2* (Figure. 4F). Comparable regulation by βOHB and Tgfb was observed in visceral progenitors, although with lesser magnitude (Figure. 4F).

We next investigated mouse fibroblast cell lines derived from *ZFP36* null (KO) or control (WT) mice [17]. Knock-out of *ZFP36* expression [33] was achieved by insertion of a neomycin cassette into the second exon of the *ZFP36* gene, leading to the synthesis of a non-functional *ZFP36 fusion* mRNA detected at high levels in KO compared to WT cells (Figure. 4G), in accordance with previously reported *ZFP36* autoregulation. In favour of a direct control of *Fn1* mRNA abundance by *ZFP36*, *Fn1* was upregulated in KO versus WT cells (Figure. 4H). However, *Ctgf* and *Loxl2* mRNAs were strongly suppressed in the KO fibroblasts (Figure. 4H).

We then performed *ZFP36* knock-down in primary subcutaneous progenitors using siRNAs which also down-regulated *ZFP36l1* (Figure. 4I). βOHB was no longer able to restrain Tgfβ—mediated stimulation of *Ctgf*, *Loxl2* and *Fn1* in *ZFP36*/*ZFP36*L1 deficient progenitors (Figure. 4J). Thus, *ZFP36* expression is required for βOHB anti-fibrotic action. However, the ability of βOHB to stimulate genes associated with

beige adipogenesis was not affected in *ZFP36* deficient progenitors (Data not shown).

4. DISCUSSION

In response to nutritional and environmental cues, fat tissue is constantly remodeled, a process involving adipose progenitors dialog with mature adipocytes and other immune cell actors, to modulate adipogenesis or tissue fibro-inflammation. Our study documents a reciprocal cross talk between brown-like adipogenesis and fibrogenic activation of progenitors. We show that metabolites promoting brown-like fat cell development might also alleviate AT responses to profibrotic Tgfβ, suggesting potential targeted approaches to reduce AT fibrosis development. First, mirroring previously reported improvement of metabolic health by adipose tissue thermogenic activation in rodents [5,6], we show here that raising mice at thermoneutrality to induce thermogenic dormancy further aggravates AT fibrotic response to HFD. We demonstrate that β-hydroxybutyrate, a metabolite able to activate brown-like adipogenesis, can also counteract Tgfβ-dependent profibrotic responses in primary cultured progenitors. We identified different pathways that underline this cross talk, governed by tissue origin of adipose progenitors (visceral or subcutaneous). In visceral progenitors, βOHB downregulates the expression and phosphorylation of Smads downstream of Tgfβ receptor activation, whereas in subcutaneous preadipocytes, βOHB is found to promote post-transcriptional regulation of Tgfβ gene targets notably through induction of *ZFP36*/Tristetraprolin, a protein regulating mRNA destabilisation. The mechanism by which BOHB exerts its anti-fibrotic effect might be accounted for its property as a signalling molecule or a metabolic substrate. As such, intracellular import of ketone bodies by monocarboxylate transporters is shared with that of lactate, and lactate fluxes are important players in beige adipocyte phenotype [34].

Importantly, our *in vitro* observations may have translational relevance since circulating β-hydroxybutyrate levels in patients with obesity inversely associate with subcutaneous adipose tissue fibrosis. β-hydroxybutyrate is a circulating metabolite that increases during ketogenesis [35], a fasting-dependent pathway. It is mainly produced by the liver as a product of partial fatty acids oxidation; however, adipose tissue was recently established as an alternative source. In particular, mature adipocytes were found to produce β-hydroxybutyrate within the AT local microenvironment, which was shown to directly impact tissue progenitors towards brown-like fat cell differentiation [23]. Importantly, we show here that in the presence of Tgfβ, although βOHB was ineffective in maintaining brown-like fat cell orientation (Figure. 2AB), it could efficiently counteract the induction of ECM genes. This suggests that raising βOHB in the obese AT context might have some interest against fibrosis development. Interestingly, a new class of anti-diabetic drugs designed to promote glucose renal excretion, referred to as "SGLT2 inhibitors" were shown to increase β-hydroxybutyrate levels in mouse models [36]. The possibility that beneficial metabolic effects of these drugs could be partly mediated by beta-hydroxybutyrate-dependent remodeling of adipose tissue is an interesting perspective that remains to be explored.

We identified the RNA binding protein *ZFP36*/Tristetraprolin as a mediator of the anti-fibrotic effect of β-hydroxybutyrate. *ZFP36* is considered a broad anti-inflammatory molecule, acting on post-transcriptional regulation of many immune-related genes by decreasing the stability of corresponding mRNAs [37–39]. *ZFP36*/Tristetraprolin null mice suffer from hyper-inflammation associated with cachexia, arthritis and dermatitis, which can be prevented by treatment with anti-TNFα antibodies [33]. Conversely, it was also demonstrated that increased Tristetraprolin expression could protect mice against immune-mediated inflammatory pathologies [40]. We report the induction of *ZFP36* gene expression by βOHB, and its downregulation by Tgfβ, along with changes in Tgfβ- or βOHB-mediated fibrotic responses of progenitors. The present study extends the spectrum of *ZFP36* targets to several Tgfβ-regulated mRNAs. Among those, *Ctgf* induced by the canonical Tgf-β/Smad pathway [41], is a crucial downstream effector in mediating Tgfβ-related fibrogenesis [42]. Its inhibition might not only prevent but also reverse fibrosis progression [43]. Based on its broad actions, *ZFP36* has great potential to impact the progenitor niche towards attenuation of ECM gene program and concomitant reduction in inflammation [44]. In accordance with the present findings that *ZFP36* expression dampens adipose progenitor response to profibrotic Tgfβ, several reports have associated *ZFP36*/Tristetraprolin deficiency with liver fibrosis aggravation [45], or its overexpression to protection against lung fibrosis following ischemia/reperfusion [46]. In the colonic epithelium, *ZFP36* was also shown to target *iNos* mRNA [47], an important mediator in fibro-inflammation regulated by Tnfα. Recently, the turnover of the peptide hormone FGF21 was found to be directly regulated by *ZFP36* family members in the context of alcoholic [48] or non-alcoholic hepatic steatosis [49], which extends the spectrum of *ZFP36* targets to metabolic regulation. Thus, the *ZFP36* family has great potential as a multi-faced post-transcriptional regulator coordinating inflammation, extracellular matrix composition and metabolic responses.

ACKNOWLEDGEMENTS

The authors wish to thank Dr. Florence Marchelli (Centre de recherche Nutrition Humaine, CRNH, Ile de France and Assistance Publique Hôpitaux de Paris), who contributed to clinical and biological data collections in patients and data base constitution. The authors thank Prof Jean-Michel Oppert, Christine Poitou and Judith Aron-Wisnewsky for his contribution to patient recruitment and the paramedic staff from the Nutrition department, Pitié-Salpêtrière hospital. The investigation was performed at Clinical Center of Human Nutrition (Paris-Ile de France). This work was supported by National Agency of Research (Captor), Fondation pour la Recherche Medicale, and EFSD/Lilly research grant. WSL and PJB are supported in part by the Intramural Research Program of the NIEHS, NIH.

CONFLICT OF INTERESTS

None declared.

APPENDIX A. SUPPLEMENTARY DATA

Supplementary data to this article can be found online at https://doi.org/10.1016/j.molmet.2022.101512.

REFERENCES

[1] Olefsky, J.M., Glass, C.K., 2010. Macrophages, inflammation, and insulin resistance. Annual Review of Physiology 72(1):219–246.

[2] Sun, K., Tordjman, J., Clément, K., Scherer, P.E., 2013. Fibrosis and adipose tissue dysfunction. Cell Metabolism 18(4):470–477.

[3] Divoux, A., Tordjman, J., Lacasa, D., Veyrie, N., Hugol, D., Aissat, A., et al., 2010. Fibrosis in human adipose tissue : composition , distribution , and link with lipid metabolism and fat. Diabetes 59:2817–2825.

[4] Marcelin, G., Ferreira, A., Liu, Y., Atlan, M., Aron-Wisnewsky, J., Pelloux, V., et al., 2017. A pdgfrα-mediated switch toward CD9highAdipocyte progenitors controls obesity-induced adipose tissue fibrosis. Cell Metabolism 25(3):673–685.

[5] Hasegawa, Y., Ikeda, K., Chen, Y., Alba, D.L., Stifler, D., Shinoda, K., et al., 2018 Jan. Repression of adipose tissue fibrosis through a PRDM16-GTF2IRD1 complex improves systemic glucose homeostasis. Cell Metabolism 27(1): 180–194.e6.

[6] Marcelin, G., Da Cunha, C., Gamblin, C., Suffee, N., Rouault, C., Leclerc, A., et al., 2020. Autophagy inhibition blunts PDGFRA adipose progenitors' cell-autonomous fibrogenic response to high-fat diet. Autophagy, 1–11. Jan 28.

[7] Becher, T., Palanisamy, S., Kramer, D.J., Eljalby, M., Marx, S.J., Wibmer, A.G., et al., 2021. Brown adipose tissue is associated with cardiometabolic health. Nat Med 27(1):58–65.

[8] Chondronikola, M., Volpi, E., Børsheim, E., Porter, C., Annamalai, P., Enerbäck, S., et al., 2014. Brown adipose tissue improves whole-body glucose homeostasis and insulin sensitivity in humans. Diabetes 63(12):4089–4099.

[9] Herz, C.T., Kulterer, O.C., Prager, M., Schmöltzer, C., Langer, F.B., Prager, G., et al., 2022. Active brown adipose tissue is associated with a healthier metabolic phenotype in obesity. Diabetes 71:93–103.

[10] Czech, M.P., 2020. Mechanisms of insulin resistance related to white, beige, and brown adipocytes. Molecular Metabolism 34:27–42. January.

[11] Kajimura, S., Spiegelman, B.M., Seale, P., 2015 Oct. Brown and beige fat: physiological roles beyond heat generation. Cell Metabolism 22(4):546–559.

[12] Berry, R., Rodeheffer, M.S., 2013. Characterization of the adipocyte cellular lineage in vivo. Nature Cell Biology 15(3):302–308.

[13] Wang, W., Ishibashi, J., Trefely, S., Shao, M., Cowan, A.J., Sakers, A., et al., 2019. A PRDM16-driven metabolic signal from adipocytes regulates precursor cell fate. Cell Metabolism 30(1):174–189.e5.

[14] Lee, M.J., 2018. Transforming growth factor beta superfamily regulation of adipose tissue biology in obesity. Biochimica et Biophysica Acta - Molecular Basis of Disease 1864(4):1160–1171.

[15] Gao, Z., Daquinag, A.C., Fussell, C., Zhao, Z., Dai, Y., Rivera, A., et al., 2020. Age associated telomere attrition in adipocyte progenitors predisposes to metabolic disease. Nat Metab 2(12):1482–1497.

[16] Lassen, P.B., Charlotte, F., Liu, Y., Bedossa, P., Le Naour, G., Tordjman, J., et al., 2017. The fat score, a fibrosis score of adipose tissue: predicting weight-loss outcome after gastric bypass. J Clin Endocrinol Metab 102(7): 2443–2453.

[17] Lai, W.S., Parker, J.S., Grissom, S.F., Stumpo, D.J., Blackshear, P.J., 2006 Dec. Novel mRNA targets for tristetraprolin (TTP) identified by global analysis of stabilized transcripts in TTP-deficient fibroblasts. Molecular and Cellular Biology 26(24):9196–9208.

[18] Soussi, H., Reggio, S., Alili, R., Prado, C., Mutel, S., Pini, M., et al., 2015. DAPK2 downregulation associates with attenuated adipocyte autophagic clearance in human obesity. Diabetes 64(10):3452–3463.

[19] Schwalie, P.C., Dong, H., Zachara, M., Russeil, J., Alpern, D., Akchiche, N., et al., 2018. A stromal cell population that inhibits adipogenesis in mammalian fat depots. Nature 559(7712):103–108.

[20] Burl, R.B., Ramseyer, V.D., Rondini, E.A., Pique-Regi, R., Lee, Y.H., Granneman, J.G., 2018. Deconstructing adipogenesis induced by β3-adrenergic receptor activation with single-cell expression profiling. Cell Metabolism, 1–10.

[21] Merrick, D., Sakers, A., Irgebay, Z., Okada, C., Calvert, C., Morley, M.P., et al., 2019. Identification of a mesenchymal progenitor cell hierarchy in adipose tissue. Science (80-) 364(6438).

[22] Polański, K., Young, M.D., Miao, Z., Meyer, K.B., Teichmann, S.A., Park, J.-E., 2020 Feb. BBKNN: fast batch alignment of single cell transcriptomes. Bioinformatics 36(3):964–965.

[23] Wang, W., Ishibashi, J., Trefely, S., Shao, M., Cowan, A.J., Sakers, A., et al., 2019. A PRDM16-driven metabolic signal from adipocytes regulates precursor cell fate. Cell Metab [Internet] 30(1):174–189.e5. https://doi.org/10.1016/j.cmet.2019.05.005. Available from:

[24] Marcelin, G., Gautier, E.L., Clément, K., 2022 Feb. Adipose tissue fibrosis in obesity: etiology and challenges. Annual Review of Physiology 84:135–155.

[25] Wang, W., Seale, P., 2016. Control of brown and beige fat development. Nature Reviews Molecular Cell Biology 17(11):691–702.

[26] Iwayama, T., Steele, C., Yao, L., Dozmorov, M.G., Karamichos, D., Wren, J.D., et al., 2015. PDGFRalpha signaling drives adipose tissue fibrosis by targeting progenitor cell plasticity. Genes & Development 29:1106–1119.

[27] Petrus, P., Lecoutre, S., Dollet, L., Wiel, C., Sulen, A., Gao, H., et al., 2020. Glutamine links obesity to inflammation in human white adipose tissue. Cell Metabolism 31(2):375–390.e11.

[28] Derynck, R., Budi, E.H., 2019. Specificity, versatility, and control of TGF-b family signaling. Science Signaling 12(570).

[29] Chang, C., 2016. Agonists and antagonists of TGF- b family. Cold Spring Harbor Perspectives in Biology, 1–52.

[30] Saini, Y., Chen, J., Patial, S., 2020. The tristetraprolin family of RNA-binding proteins in cancer: progress and future prospects. Cancers 12(6):1–21.

[31] Bakheet, T., Hitti, E., Khabar, K.S.A., 2018. ARED-Plus: an updated and expanded database of AU-rich element-containing mRNAs and pre-mRNAs. Nucleic Acids Research 46(D1):D218–D220.

[32] Moore, M.J., Blachere, Nathalie E., Fak CYP, John J., Sawicka, Kirsty, Parveen, Salina, et al., 2018. *ZFP36* RNA-binding proteins restrain T cell activation and anti-viral immunity. Elife 7:e33057, 2018;7:e33057.

[33] Taylor, G.A., Carballo, E., Lee, D.M., Lai, W.S., Thompson, M.J., Patel, D.D., et al., 1996. A pathogenetic role for TNFα in the syndrome of cachexia, arthritis, and autoimmunity resulting from tristetraprolin (TTP) deficiency. Immunity 4(5):445–454.

[34] Lagarde, D., Jeanson, Y., Barreau, C., Moro, C., Peyriga, L., Cahoreau, E., et al., 2021. Lactate fluxes mediated by the monocarboxylate transporter-1 are key determinants of the metabolic activity of beige adipocytes. Journal of Biological Chemistry 296(17):100137.

[35] Newman, J.C., Verdin, E., 2017. β-Hydroxybutyrate: a signaling metabolite. Annual Review of Nutrition 37:51–76.

[36] Kim, J.H., Lee, M., Kim, S.H., Kim, S.R., Lee, B.-W., Kang, E.S., et al., 2019 Apr. Sodium-glucose cotransporter 2 inhibitors regulate ketone body metabolism via inter-organ crosstalk. Diabetes, Obesity and Metabolism 21(4):801–811.

[37] Fu, M., Blackshear, P.J., 2017. RNA-binding proteins in immune regulation: a focus on CCCH zinc finger proteins. Nature Reviews Immunology 17(2):130–143.

[38] Anderson, P., 2008. Post-transcriptional control of cytokine production. Nature Immunology 9(4):353–359.

[39] Hikichi, Y., Motomura, Y., Takeuchi, O., Moro, K., 2021 Dec. Post-transcriptional regulation of ILC2 homeostatic function via tristetraprolin. Journal of Experimental Medicine 218(12).

[40] Patial, S., Curtis, A.D., Lai, W.S., Stumpo, D.J., Hill, G.D., Flake, G.P., et al., 2016 Feb 16. Enhanced stability of tristetraprolin mRNA protects mice against immune-mediated inflammatory pathologies. Proceedings of the National Academy of Sciences 113(7), 1865 LP – 1870.

[41] Duncan, M.R., Frazier, K.S., Abramson, S., Williams, S., Klapper, H., Huang, X., et al., 1999 Oct. Connective tissue growth factor mediates transforming growth factor beta-induced collagen synthesis: down-regulation by cAMP. FASEB J Off Publ Fed Am Soc Exp Biol 13(13):1774–1786.

[42] Mori, T., Kawara, S., Shinozaki, M., Hayashi, N., Kakinuma, T., Igarashi, A., et al., 1999 Oct. Role and interaction of connective tissue growth factor with transforming growth factor-beta in persistent fibrosis: a mouse fibrosis model. Journal of Cellular Physiology 181(1):153–159.

[43] Lipson, K.E., Wong, C., Teng, Y., Spong, S., 2012. CTGF is a central mediator of tissue remodeling and fibrosis and its inhibition can reverse the process of fibrosis. Fibrogenesis & Tissue Repair 5(S1):2–9.

[44] Wynn, T.A., Ramalingam, T.R., 2012. Mechanisms of fibrosis: therapeutic translation for fibrotic disease. Nat Med 18(7):1028–1040.

[45] Wu, J.C., Luo, S.Z., Liu, T., Lu, L.G., Xu, M.Y., 2019. Linc-SCRG1 accelerates liver fibrosis by decreasing RNA-binding protein tristetraprolin. The FASEB Journal 33(2):2105–2115.

[46] Cao, Y., Huang, W., Wu, F., Shang, J., Ping, F., Wang, W., et al., 2021 Jul. *ZFP36* protects lungs from intestinal I/R-induced injury and fibrosis through the CREBBP/p53/p21/Bax pathway. Cell Death & Disease 12(7):685.

[47] Eshelman, M.A., Matthews, S.M., Schleicher, E.M., Fleeman, R.M., Kawasawa, Y.I., Stumpo, D.J., et al., 2019. Tristetraprolin targets Nos2 expression in the colonic epithelium. Scientific Reports 9(1):1—13.

[48] Bathula, C.S., Chen, J., Kumar, R., Blackshear, P.J., Saini, Y., Patial, S., 2022. *ZFP36*L1 regulates Fgf21 mRNA turnover and modulates alcoholic hepatic steatosis and inflammation in mice. American Journal Of Pathology 192(2):208—225.

[49] Sawicki, K.T., Chang, H.-C., Shapiro, J.S., Bayeva, M., De Jesus, A., Finck, B.N., et al., 2018 Jul. Hepatic tristetraprolin promotes insulin resistance through RNA destabilization of FGF21. JCI insight 3(13).

